*Annalen der Physik*

annalen der physik
www.ann-phys.org

PERSPECTIVE OPEN ACCESS

# Coupled Dynamics Between Networks and Fields in Physical Space: A Theoretical Perspective

Alex Arenas[1,2] | Oriol Artime[3,4] | Albert Díaz-Guilera[3,4] | Sergio Gómez[1,2] | Clara Granell[1,2]

[1]Departament d'Enginyeria Informàtica i Matemàtiques, Universitat Rovira i Virgili, Tarragona, Spain | [2]Center for Computational Science and Applied Mathematics (ComSCIAM), Universitat Rovira i Virgili, Tarragona, Spain | [3]Departament de Física de la Matèria Condensada, Universitat de Barcelona, Barcelona, Spain | [4]Universitat de Barcelona Institute of Complex Systems (UBICS), Universitat de Barcelona, Barcelona, Spain

**Correspondence:** Alex Arenas (alexandre.arenas@urv.cat)

**Received:** 29 May 2026 | **Revised:** 27 August 2026 | **Accepted:** 1 September 2026

**Keywords:** continuum–discrete dynamics | network–field coupling | spatially embedded networks

## ABSTRACT

Many complex systems cannot be understood from network structure alone, nor from continuum descriptions in isolation, because their dynamics emerge from the reciprocal coupling between discrete interaction architectures and spatially extended physical fields. This perspective article surveys mathematical and computational frameworks for such network–field systems, focusing on models in which a graph is either itself the spatial substrate of a field or is embedded in a surrounding medium that mediates transport, signaling, forcing, or spatially distributed hazards. We first introduce a unified formalism for bidirectionally coupled network–field dynamics, emphasizing observation and injection operators that link node variables to continuum processes while preserving balance laws. We then examine two major modeling classes: fields evolving directly on metric graphs, where partial differential equations are posed on network geometries with vertex matching conditions; and hybrid discrete–continuous systems, where node dynamics are coupled to fields in the ambient domain, with particular attention to port-Hamiltonian formulations that provide energy-consistent interconnection principles. Within this common framework, we discuss representative modeling applications in neurobiology, including diffusion-mediated cellular communication and extracellular neural signaling, and in infrastructure systems, where network functionality depends on spatially distributed flows, loads, and hazards. Across these examples, a common picture emerges: the field is not merely an external environment, but an active dynamical layer that reshapes effective interactions, timescales, and collective behavior. By synthesizing concepts that are often developed separately across disciplines, this perspective article aims to clarify the mathematical structure, physical interpretation, and numerical challenges of coupled network–field models, and to highlight their role as a unifying language for spatially embedded complex systems.

## 1 | Introduction

Spatial embedding becomes dynamically relevant whenever the medium carries signals, fluxes, forces, or hazards on timescales comparable to those of the discrete units. In such cases, the embedding domain is not only a geometric constraint on the network: it supplies additional dynamical degrees of freedom that can mediate interactions, impose constraints, and modify collective response. As a result, system-level behavior emerges from the interplay between dynamics on the network and processes unfolding in the surrounding medium [1–4].

This situation arises in a wide range of contexts. In neurobiology, neuronal and glial interactions are shaped not only by synaptic connectivity but also by extracellular ionic concentrations, electric fields, and diffusing neuromodulators [5–8]. In

engineered infrastructures, the functionality of transportation, power, or water-distribution networks depends on spatially distributed loads, flows, and hazards that cannot be represented as purely topological perturbations [9–11]. Across these examples, the network both constrains and responds to spatial processes, giving rise to genuinely coupled network–field dynamics.

Traditional modeling approaches often privilege one of these two levels of description. Purely graph-based models are well suited to characterize connectivity, heterogeneity, modularity, and interdependence, but they generally neglect the spatially extended mechanisms through which interactions are mediated, modulated, or transported. Conversely, continuum descriptions capture diffusion, flow, wave propagation, or field-mediated communication, yet they often coarse-grain away the discrete architecture through which localized exchange, routing, or coordination occur. For many systems of current interest, neither description is sufficient in isolation.

These limitations have motivated the development of some mathematical and computational frameworks that explicitly couple discrete networks to continuous spatial dynamics. Depending on the application and scale of interest, such frameworks take the form of partial differential equations posed on metric graphs, node–field PDE–ODE systems [12], or multiscale schemes that exchange mass, fluxes, or forcing between discrete and continuum representations [13]. Although these approaches have emerged in different disciplines and under different terminologies, they address a common problem: how to represent, analyze, and simulate systems in which network structure and spatial fields are dynamically interdependent.

Here we survey the main formalisms for such network–field coupling in physical space. A useful distinction must be made at the outset between two broad classes of network–field models. In the first class, the network itself constitutes the spatial support of the field: the relevant dynamics are posed directly on a metric graph, with edgewise partial differential equations and vertex matching conditions determining transport, diffusion, or wave propagation. In the second class, the network is embedded in an ambient continuum, so that discrete node variables interact with one or more fields defined on a surrounding domain through observation, forcing, exchange, or boundary operators. Both classes fit naturally within a common network–field perspective, in the sense that system-level behavior emerges from the reciprocal interplay between discrete interaction structure and spatially extended processes. However, they differ fundamentally in the geometry of the field support, in the role played by node variables, and in the mathematical issues that govern analysis and simulation. In what follows, we use this distinction to organize the perspective article and to clarify which aspects of the proposed notation are genuinely shared across modeling frameworks and which are specific to a given class of systems. We close the introduction by making explicit the three contributions of this Perspective. First, we distinguish two mathematically different but conceptually related classes of network–field systems: fields evolving directly on metric graphs and discrete networks embedded in ambient continua. Second, we introduce an operator-level notation based on observation and injection maps, which makes explicit how node variables and spatial fields are coupled. Third, we emphasize physical consistency as a criterion for constructing meaningful coupled models, with particular attention to balance laws, passivity, and energy- or mass-preserving interconnection principles. Taken together, these elements provide a structural language for comparing network–field systems across domains, without reducing them to either purely graph-based dynamics or purely continuum descriptions.

## 2 | Mathematical Notation

This section introduces a unified mathematical framework for network–field coupling. Rather than serving only as notation, it provides a general operator-based formulation that captures the essential structure of bidirectionally coupled discrete–continuous systems. In this way, it both enables systematic comparison across previously disconnected approaches and supplies a common formal backbone for the diverse application-specific models discussed below. We consider systems in which a discrete interaction structure (a graph) is embedded in a continuous domain and coupled to one or more fields evolving over that domain. Let $G = (V, E)$ be a graph with $|V| = N$ nodes, adjacency matrix $A = (A_{ij})$, node states $x_i(t)$, and node positions $\mathbf{r}_i \in \Omega \subset \mathbb{R}^d$. Let $u(\mathbf{r}, t)$ denote a continuum field (scalar or vector) defined on $\Omega$. Hybrid discrete–continuous models specify (i) dynamics on the graph and (ii) field dynamics on $\Omega$ (with appropriate initial/boundary conditions), together with coupling operators that map field information to nodes, $\mathcal{M}_i[u](t)$ (e.g., point evaluation $u(\mathbf{r}_i, t)$, local averages, or gradients), and node/edge activity back to the field (e.g., via source/sink or boundary terms). A generic bidirectionally coupled network–field model can be written as

$$\dot{x}_i = F_i(x_i) + \sum_{j=1}^{N} A_{ij}\, G_{ij}(x_i, x_j) + \Phi_i(\mathcal{M}_i[u](t), x_i), \tag{1}$$

$$\mathcal{T} u(\mathbf{r}, t) = \mathcal{L} u(\mathbf{r}, t) + \Psi\big(\mathbf{r}, u; \{\mathbf{r}_i, x_i\}_{i=1}^{N}\big), \tag{2}$$

where we have introduced the general linear temporal operator

$$\mathcal{T} = a_2(\mathbf{r}, t)\partial_t^2 + a_1(\mathbf{r}, t)\partial_t + a_0(\mathbf{r}, t). \tag{3}$$

Moreover, $\mathcal{L}$ is a differential operator on $\Omega$ and $\Psi$ encodes how discrete degrees of freedom act on the field (e.g., localized forcing or boundary constraints), while $\Phi_i$ articulates how the medium affects the states of the nodes. The admissibility of the observation operators $\mathcal{M}_i$ depends on the regularity class in which the field $u$ is posed. In particular, point evaluation at $\mathbf{r}_i$ requires sufficient regularity for $u(\mathbf{r}_i, t)$ to be well defined, while singular node-to-field couplings may require weak formulations or regularization. Thus, the operators $\mathcal{M}_i$ and $\Psi$ should be understood as model-dependent interconnection maps whose analytical status must be checked in the relevant functional setting.

The notation in Equation (2) also allows for the possibility that the field and node dynamics evolve on markedly different temporal scales. In many applications, the continuum relaxes much faster than the discrete variables, or conversely acts as a slow background that modulates comparatively rapid node dynamics. Such scale separation can justify reduced descriptions

in which the field is eliminated in favor of an effective interaction kernel or memory term acting on the network variables. However, this reduction is not generic: it requires identifiable asymptotic regimes, such as fast diffusion, rapid local equilibration, or other singular-perturbation limits, together with assumptions ensuring that the reduced coupling remains well defined. In the absence of such conditions, the full coupled node–field dynamics must be retained, and the effective interaction structure cannot in general be inferred from topology alone.

Equations (1)–(2) are introduced here as a common formal template for coupled network–field dynamics, not as a claim that every such system can be treated within a single abstract setting without further qualification. A concrete model is obtained only after specifying the state spaces of $x_i$ and $u$, the domain and regularity of the differential operator $\mathcal{L}$, and the admissible observation and injection maps that realize the coupling between discrete and continuous degrees of freedom. Depending on the application, these maps may involve point evaluation, local averaging, fluxes, boundary traces, or singular source terms, and the analytical status of the resulting system depends critically on these choices. The notation therefore serves primarily as a structural language for comparison across model classes, while existence, uniqueness, regularity, and physical interpretation remain specific to the chosen realization.

For classes of models in which the coupling represents exchange of a conserved extensive quantity, the node and field terms should satisfy an appropriate global balance law, up to boundary fluxes, distributed sources, and external forcing. A schematic example is obtained when $x_i$ denotes a nodal amount of some stored quantity and $w_i > 0$ is the corresponding conversion factor, so that

$$\frac{d}{dt}\left(\sum_{i=1}^{N} w_i x_i + \int_{\Omega} u(\mathbf{r},t)\,d\mathbf{r}\right) = \text{boundary fluxes} + \text{distributed sources/sinks} + \text{external forcing}.$$

This expression is intended only as a structural prototype. Its precise physical meaning depends on the dimensions assigned to $x_i$, $u$, and $w_i$, and on whether the quantity being exchanged is mass, charge, probability, energy, or another conserved observable. In particular, balance laws for stored quantity should be distinguished from energy balances, which generally involve different constitutive definitions and, in dissipative systems, additional loss terms. The main point is therefore not that all coupled network–field systems obey a single universal conservation formula, but that in physically consistent realizations the coupling operators must be chosen so that the relevant balance structure is respected.

The purely networked setting is recovered from Equations (1)–(2) by setting $\Phi_i \equiv 0$ and removing the field equation; conversely, common hybrid models correspond to specific choices of $(\mathcal{L}, \mathcal{M}_i, \Phi_i, \Psi)$. For later reference, Table 1 summarizes how the main model classes discussed in this perspective article instantiate the generic operators of Equations (1)–(2), together with the principal timescale assumptions and analytical issues associated with each setting.

**TABLE 1** | Representative instantiations of the generic network–field formalism introduced in Equations (1)–(2). For each example, the table indicates the spatial support of the field, the nature of node variables, the observation and coupling operators, and the principal analytical or numerical challenges. The table is intended as a roadmap for the applications discussed later: metric-graph models are treated in Section 3, and neurobiological and infrastructure examples in Section 5.

| Example | Support | Field $u$ | Node state $x_i$ | Observation operators $\mathcal{M}_i$ | Couplings $\Phi_i, \Psi$ | Key issue |
|---|---|---|---|---|---|---|
| Metric-graph PDEs | Metric graph $\Gamma$ | $u_e(s,t)$ | Usually absent explicitly | Implicit through vertex matching | Coupling through continuity / flux conditions | Vertex conditions, spectral structure, localization |
| Circadian model | Ambient continuum | $A(\mathbf{r},t)$ | $X_i = (x_i, y_i)$ | $A(\mathbf{r}_i,t)$ | $\Phi_i = g(A(\mathbf{r}_i,t))$, $\Psi = \sum_j h(X_j)\delta(\mathbf{r}-\mathbf{r}_j)$ | Point sources, fast-diffusion reduction |
| Extracellular neural tissue | Ambient continuum | $[K^+]_e(\mathbf{r},t)$, etc. | Neuronal state variables | Local field sensing | Field-modulated excitability and localized release | Multiscale stiffness, singular forcing |
| Infrastructure/hazards | Spatial embedding domain | Flood/stress/hazard field | Operational asset state | Local value or average | Hazard-induced degradation and localized exchange | Thresholds, uncertainty, coupled simulation |

Note that in the present formulation, the network architecture is assumed to be fixed: the adjacency matrix is treated as quenched and does not adapt to the state of the surrounding medium. Likewise, the parameters entering the local and interaction terms are taken to be time-independent unless stated otherwise. This restriction excludes adaptive or coevolving network–field systems, in which the interaction architecture or the dynamical parameters may themselves evolve in response to the field. We adopt this assumption to isolate the consequences of discrete–continuous coupling at fixed architecture, while noting that both topology and dynamical parameters are known to play distinct and often intertwined roles in shaping collective behavior on networks [14].

## 3 | Fields on Networks: Dynamics on Metric Graphs

In some systems, the physically relevant space is not the surrounding bulk medium but the network geometry itself. In this case, transport, diffusion, or wave propagation occur in a branched one-dimensional domain, and the network acts simultaneously as the interaction architecture and spatial support for the field. In the metric-graph setting, one should distinguish between models in which the dynamics are carried entirely by edgewise fields and models in which additional vertex degrees of freedom are introduced explicitly. The examples emphasized in this section belong mainly to the first category: the network serves as the geometric support of the continuum, and the vertices enter through continuity, flux balance, or other matching conditions rather than through independent state variables. More general graph-supported models may augment this structure with dynamical variables at the vertices, dynamic boundary conditions, or storage and dissipation mechanisms localized at junctions. Our purpose here is not to survey that full generality, but to isolate the canonical case in which the field evolves directly on the network geometry itself.

For models posed directly on network geometries, the spatial support of the field is not a bulk domain $\Omega \subset \mathbb{R}^d$ but a metric graph $\Gamma = (V, E)$, where each edge $e \in E$ is identified with an interval $[0, \ell_e]$. The field is then written as $u = \{u_e(s,t)\}_{e\in E}$, with $s$ the edge-wise coordinate, and evolves according to an operator $\mathcal{L}_\Gamma$ acting on each edge together with matching conditions at vertices. A prototypical class of PDEs on metric graphs arises when signals, vibrations, or waves propagate along the edges of a networked structure, such as transmission lines, elastic strings, or branched waveguides. A minimal model is then the wave equation

$$\partial_t^2 u_e = c_e^2 \partial_s^2 u_e, \qquad s \in (0, \ell_e),$$

where $c_e$ denotes the propagation speed on edge e. This represents a partial differential equation for each edge, supplemented by continuity of $u$ and Kirchhoff flux conservation at each vertex (i.e., $\sum \partial_s u_e(v) = 0$ if all $c_e$ are equal). In this class of models, the network acts simultaneously as interaction architecture and spatial domain.

Vertex conditions are not a mere technicality: they determine the domain of the differential operator on the metric graph, and hence its spectrum, self-adjointness, and the physical behavior at junctions. Continuity together with Kirchhoff flux balance (the standard Neumann–Kirchhoff conditions) guarantees conservation of mass or energy at vertices, but other choices—Dirichlet, $\delta$-type, or Robin conditions—arise in applications involving clamped junctions, localized potentials, or reactive boundaries. Each choice alters wave scattering and transport properties, and can fundamentally affect phenomena such as eigenmode localization or synchronization thresholds.

A canonical example of a field posed directly on a network geometry is provided by the metric-graph framework developed by Brio, Caputo, and Kravitz [15]. In their work, they develop and compare three numerical routes for linear PDEs on metric graphs with continuity and Kirchhoff vertex conditions: a spectral method based on the generalized graph Laplacian, a second-order finite-difference scheme, and a discontinuous Galerkin formulation. Their main conclusion is that the spectral approach is the natural tool for linear problems on metric graphs: once the eigenvectors and eigenvalues of the generalized Laplacian are computed, Helmholtz, Poisson, and wave-type equations reduce to mode-by-mode evolution, exactly as in classical Fourier analysis on an interval. Their work establishes the generalized Laplacian as the central computational object for PDEs posed directly on network geometries and shows that spectral decompositions provide the cleanest framework for linear dynamics, although extensions to non-Kirchhoff or non-self-adjoint settings are substantially more delicate.

Note that in this context, the generalized graph Laplacian is the metric-graph Laplacian: it acts as the one-dimensional second-derivative operator on each edge, while its domain is defined by continuity and Kirchhoff flux-balance conditions at the vertices. It is therefore a differential operator on the graph geometry, not the combinatorial Laplacian matrix of an abstract graph.

The above spectral decomposition in which the generalized graph Laplacian is diagonalized to reduce linear PDEs on metric graphs to mode-by-mode evolution, provides the natural setting for studying wave localization. Building on this framework, Kravitz, Brio and Caputo [16] further showed that exactly localized eigenmodes are non-generic and arise only under precise resonance conditions relating edge lengths within specific subgraphs such as triangles, quadrilaterals, and pumpkin configurations. They also demonstrated that these localized modes can dominate the asymptotic response of the wave equation and proposed intrinsic energy-density based criteria to quantify localization independently of edge lengths; see Figure 1. From an applied viewpoint, localized resonant modes imply that wave energy may accumulate on a small subset of edges instead of being distributed across the whole network. For example, in electrical grids they found that even approximately localized eigenmodes can produce damaging loads on equipment, suggesting that reinforcement should focus on the regions where these modes attain their largest amplitudes.

This sequence of contributions culminates in the broader synthesis of Böttcher and Porter [17] offering a methodological and conceptual framework for PDEs on metric networks, framing them as a natural extension of conventional network dynamics when edgewise spatial structure cannot be neglected. In their formulation, each edge carries a real interval, so that the network

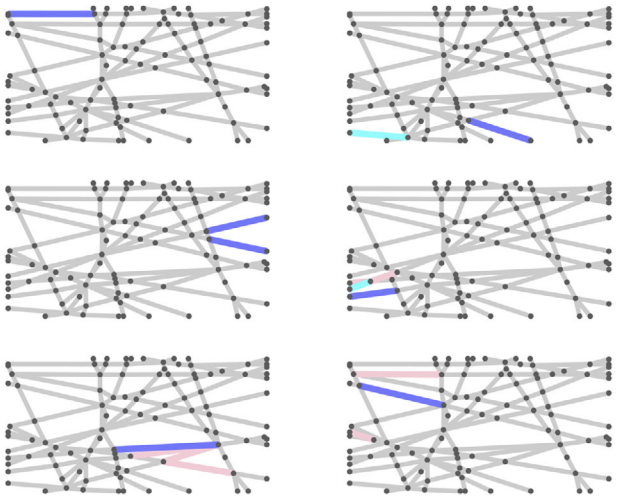

**FIGURE 1** | Buffon's needle graph with 104 vertices and 165 arcs, embedded in the planar domain $[0, 200] \times [0, 200]$. The panels show the approximately localized eigenvectors $V_q$ for $q = 5, 8, 13, 18, 20$, and 21. For each arc $j$, the quantity $e_q(j)$, that measures the normalized $L^2$ energy of the $q$th eigenvector on edge $j$, is represented by the following color code: gray for $e_q(j) < 0.06$, pink for $0.06 \le e_q(j) < 0.12$, cyan for $0.12 \le e_q(j) < 0.2$, and blue for $e_q(j) \ge 0.2$. Reproduced with permission. [Ref. [16], Copyright 2023, Elsevier].

becomes a one-dimensional geometric domain on which one can define differential operators and study spatially extended processes such as Schrödinger, Poisson, heat, and wave equations. In the metric-network setting of Böttcher and Porter [17], the generic network–field formulation Equations (1) and (2) reduces to fields on graphs in which no independent node states are introduced. The bulk field $u(\mathbf{r}, t)$ is replaced by an edgewise field $u = \{u_e(s, t)\}_{e \in E}$ defined on the metric graph $\Gamma$, with $u_e : [0, \ell_e] \times \mathbb{R}_+ \to \mathbb{R}$, and the continuum operator $\mathcal{L}$ is replaced by a differential operator $\mathcal{L}_\Gamma$ (generalized Laplacian) acting on each edge together with continuity and boundary conditions at the vertices. In this specialization, there are no independent node variables, and the dynamics are carried entirely by the edgewise field $u$ on the metric graph

$$\partial_t u = \mathcal{L}_\Gamma u,$$

or, for second-order problems such as wave propagation,

$$\partial_t^2 u = \mathcal{L}_\Gamma u.$$

Elliptic problems such as the Poisson equation $\mathcal{L}_\Gamma \phi = \rho$ also arise naturally in this setting, alongside parabolic and hyperbolic equations. A particularly useful contribution of the paper is the explicit treatment of degenerate eigenmodes, which are linked to network symmetries and must be handled carefully in spectral computations. The authors combine spectral methods, finite-difference solvers, Weyl-law estimates, and group-theoretic arguments to show how one can reliably identify characteristic wavenumbers and their multiplicities for canonical linear PDEs on metric networks. Their numerical examples also illustrate that this framework extends beyond analytically tractable few-edge configurations: for example, Figure 2, reproduced from their Poisson problem on a metric hexagonal lattice, shows an edgewise field defined on a network with $N = 154$ nodes and $M = 213$ edges, together with finite-difference and spectral solutions that closely match the exact profile. In this way, their work complements the earlier contributions of Brio, Caputo, and Kravitz by embedding numerical spectral methods, localized eigenvectors, and related linear PDE models within a broader framework for dynamics on metric networks, while also demonstrating applicability to substantially larger graphs.

Taken together, these three recent contributions delineate a coherent progression: from numerical spectral formulations for PDEs on metric graphs, to localization phenomena in wave dynamics, and finally to a broader methodological framework for metric–network PDEs.

## 4 | Networks Embedded in Fields: Discrete Structures Coupled to Continua

We now turn to systems in which a discrete interaction network is embedded in, and dynamically coupled to, a continuous field. In contrast to the metric-graph setting of Section 3, where transport is confined to the network itself, here the nodes occupy positions in a surrounding medium $\Omega \subset \mathbb{R}^d$ and interact both through their direct network architecture and through a shared continuum. The field is therefore not just an external environment: it acts as an additional interaction channel that can mediate transport, feedback, and effective long-range couplings between nodes. This class of systems is captured by the general form introduced in Equations (1) and (2).

From a physical perspective, many mixed ODE (network)–PDE (field) systems consist of two complementary subsystems: localized components that store or process energy in a finite number of degrees of freedom, and an extended medium that transports or redistributes that energy in space. Examples include lumped electromechanical devices coupled to transmission or wave-propagation media, mechanical subsystems attached to elastic structures, and finite-dimensional controllers interconnected with reaction–diffusion, flow, or other distributed-parameter systems [18, 19]. In such situations, the central modeling requirement is not only to write evolution equations for each subsystem separately, but also to describe their interconnection in a way that respects the balance of exchanged power: energy may be transferred between discrete and distributed components, dissipated internally, or injected through boundaries and external ports, but it should not appear or disappear spuriously. From the viewpoint of complex systems, such hybrid models are particularly relevant because the continuum can reshape the effective interaction kernel of the network, thereby altering synchronization, pattern formation, spreading dynamics, and collective response.

This observation motivates the use of the port-Hamiltonian (pH) framework, which provides a systematic language to represent storage, dissipation, and interconnection on equal footing, while keeping explicit how local node dynamics and field-mediated interactions combine into a single hybrid system. Originally developed for finite–dimensional systems [20] and later extended to infinite–dimensional systems [21], the pH approach describes coupled physical systems through energy functions and geometric interconnections that preserve power balance. For mixed

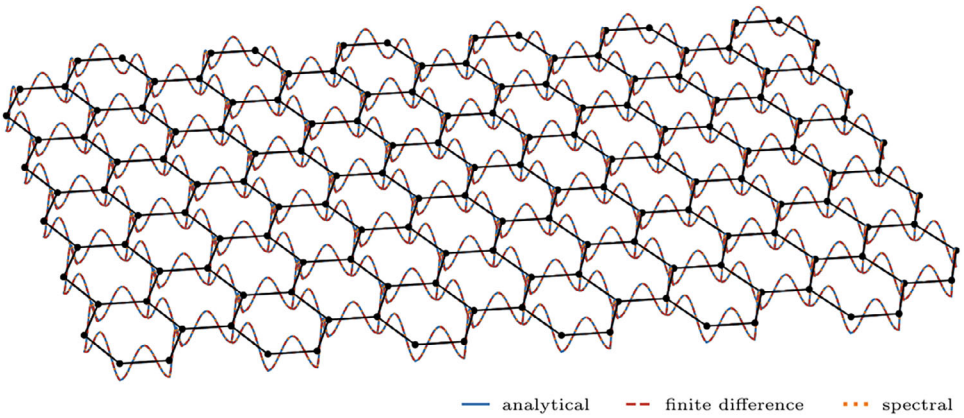


**FIGURE 2** | Poisson equation on a finite metric graph with hexagonal-lattice geometry. Each edge is treated as a one-dimensional interval endowed with Kirchhoff vertex conditions. The network consists of $N = 154$ nodes and $M = 213$ edges. The source term is prescribed edgewise, and the resulting solution is shown together with numerical approximations obtained using finite-difference and spectral methods. This example illustrates how PDE dynamics on metric networks extend naturally beyond small star-like graphs to larger geometries while retaining an edge-resolved field description. Reproduced with permission. [Ref. [17], Copyright 2025, SIAM].

ODE–PDE systems, it offers a rigorous realization of the global conservation principle noted informally in Section 2, and could be mapped to the coupling operators $\Phi_i$ and $\Psi$ in Equations (1) and (2). In the next section we will scrutinize its formulation.

### 4.1 | Port-Hamiltonian Formulation of the Component Subsystems

A useful way to organize bidirectional couplings between networked discrete units and continuous fields is the port-Hamiltonian framework; see ref. [22] for an excellent introduction to the topic. Here, a port denotes an interface through which a subsystem exchanges energy with its environment. It is characterized by a pair of conjugate variables—such as force and velocity, or voltage and current—whose product equals the instantaneous power flowing through the interface. The central physical idea is that energy serves as a common language across physical domains: discrete and distributed subsystems may be mechanical, electrical, hydraulic, or thermal, yet their interaction can still be described in terms of storage, dissipation, and power exchange. In this perspective, the essential modeling step is not only to specify each subsystem's dynamics separately, but also to define an interconnection law that accounts consistently for power flow between them. This makes the framework especially attractive for mixed ODE–PDE systems, where localized components and spatially extended media coexist, and exchange energy through interfaces. A further advantage is compositionality: power-preserving interconnections of subsystems yield a new system of the same type, allowing complex network–field models to be assembled from simpler building blocks. In network terms, this compositionality is important because it separates three ingredients that are often conflated: the intrinsic node dynamics, the direct node–node interconnection structure, and the indirect coupling mediated by the ambient field.

In the pH framework, the node dynamics are associated with a finite-dimensional Hamiltonian $H_{\text{ode}}(x)$ representing the total energy stored in the discrete components. The evolution takes the form

$$\dot{x} = \big(J(x) - R(x)\big)\nabla H_{\text{ode}}(x) + B(x)u_{\text{ode}}, \quad y_{\text{ode}} = B(x)^{\top}\nabla H_{\text{ode}}(x), \tag{4}$$

here $x$ stacks the states of the discrete network components, such as node voltages, currents, positions, or momenta. The skew-symmetric matrix $J(x) = -J(x)^{\top}$ encodes the conservative internal interconnection structure of the discrete subsystem; in networked settings, its sparsity pattern or block structure may reflect the underlying adjacency, incidence, or coupling topology. The matrix $R(x) = R(x)^{\top} \succeq 0$ represents internal dissipation, such as damping, resistance, or other irreversible losses. The matrix $B(x)$ specifies how external actuation or field-mediated signals enter the node dynamics through the ports, while the output

$$y_{\text{ode}} = B(x)^{\top}\nabla H_{\text{ode}}(x)$$

is the conjugate port variable through which the discrete subsystem returns power to its environment. The instantaneous power supplied through the port is $u_{\text{ode}}^{\top}y_{\text{ode}}$. Thus, direct graph-based interactions may already be encoded through $J$, $R$, or $H_{\text{ode}}$, while the continuum contributes an additional spatially mediated interaction channel.

For the continuum field, we consider a distributed-parameter port-Hamiltonian system defined on a spatial domain $\Omega$ with boundary $\partial\Omega$. Let $z(\mathbf{r}, t)$ be the state variables (e.g., displacement, momentum, or field intensity) and $\mathcal{H}(z)$ the Hamiltonian functional representing the energy stored in the field. Following [21], the dynamics are expressed as

$$\frac{\partial z}{\partial t} = \big(\mathcal{P} - \mathcal{R}(z)\big)\frac{\delta \mathcal{H}}{\delta z} + \mathcal{G}u_{\text{pde}}, \qquad y_{\text{pde}} = \mathcal{G}^{*}\frac{\delta \mathcal{H}}{\delta z} + \mathcal{D}u_{\text{pde}}, \tag{5}$$

where $\mathcal{P}$ is a formally skew-symmetric differential operator that generates the conservative transport or propagation part of the field dynamics, $\mathcal{R}(z)$ is a positive semidefinite dissipation operator describing distributed losses or damping, and $\mathcal{G}$ specifies how

external inputs or interconnection signals act on the continuum subsystem. The adjoint operator $\mathcal{G}^*$ extracts the corresponding output variable conjugate to that input, while $\mathcal{D}$ is a feed-through term accounting for any direct input–output contribution. In infinite-dimensional settings, however, formal skew-symmetry alone does not determine a valid evolution problem: one must also specify a suitable operator domain, state space, and boundary conditions so that the corresponding realization has the required semigroup and energy properties.

It is worth noticing that once coupled to the nodes, the field generates an additional, geometry-dependent interaction channel whose effects are generally nonlocal in space and non-instantaneous in time.

The boundary port variables $(u_{\text{pde}}, y_{\text{pde}})$ are constructed so that the energy balance satisfies

$$\frac{d}{dt}\mathcal{H} = \int_{\partial\Omega} u_{\text{pde}}^{\top} y_{\text{pde}}\, dS - \int_{\Omega} \left(\frac{\delta\mathcal{H}}{\delta z}\right)^{\top} R(z) \frac{\delta\mathcal{H}}{\delta z}\, d\mathbf{r}, \tag{6}$$

The first term represents the power exchanged with the environment through the boundary ports, while the second term accounts for internal dissipation within the distributed subsystem. Hence, in the absence of dissipation, any variation of the field energy is entirely due to power flowing across the boundary. This structure ensures that all energy exchange with the environment occurs through the boundary ports: in the absence of dissipation, any change in the field's internal energy equals the power flowing through the boundary.

Equations (4) and (5) provide a complete description of the isolated discrete and distributed subsystems. To obtain a coupled network–field model of the form shown in Equations (1)–(2), these subsystems must be interconnected in a manner that preserves overall power balance. The port-Hamiltonian formulation may be viewed as a concrete realization of the generic network–field structure introduced in Section 2. In this correspondence, the finite-dimensional state $x$ represents the discrete node variables and the distributed state $z$ represents the continuum field, possibly after rewriting the field dynamics in first-order form. The observation operators $\mathcal{M}_i$ are realized by local port maps that extract traces, fluxes, or other field observables at coupling sites, whereas the node-to-field action $\Psi$ is realized through the distributed input operators acting on the field subsystem. The field-mediated term $\Phi_i$ in the node dynamics then arises from the interconnection law itself rather than being postulated independently. This makes explicit that the port-Hamiltonian framework is a structured way of specifying the abstract operators of Equations (1)–(2).

### 4.2 | Coupling Network and Field Through Ports

In addition to the boundary ports $(u_{\text{pde}}, y_{\text{pde}})$ of the distributed parameter system in Equation (5), we consider $N$ node-associated coupling ports at positions $\mathbf{r}_i \in \Omega$, one for each node $i$ of the network. These sites anchor the discrete interaction network to the continuum and define where the field is sampled and where node-dependent forcing is injected back into the medium. Each such port is characterized by a pair of conjugate variables $(u_i, y_i)$: the output $y_i$ is obtained by evaluating a relevant field observable at $\mathbf{r}_i$ (e.g., displacement, velocity, or flux), while the input $u_i$ represents a localized action applied to the field at that same point (e.g., a point force or source). These interior ports provide the interface through which discrete nodes exchange energy with the surrounding continuum. The power-preserving interconnection between discrete and distributed subsystems is then defined by the condition that the total power flow through all interconnected ports vanishes:

$$u_{\text{ode}}^{\top} y_{\text{ode}} + \sum_{i=1}^{N} u_i^{\top} y_i = 0. \tag{7}$$

For the canonical case where each node couples exclusively to its own field port in a power-conserving manner, this relation reduces componentwise to

$$u_{\text{ode},i} = y_i, \qquad y_{\text{ode},i} = -u_i, \qquad i = 1, \ldots, N. \tag{8}$$

Under this interconnection, the continuum acts as a mediator between nodes: perturbations generated by one node propagate through the field and can influence other nodes according to the Green function, propagator, or transfer properties of the distributed subsystem. In this sense, the embedded network acquires an effective interaction layer induced by the field, which may differ substantially from the direct graph topology.

To make these localized ports explicit, we introduce two families of operators. Let $\mathcal{M}_i$ denote the observation map that extracts the relevant field observable at $\mathbf{r}_i$ from the distributed state $x_{\text{pde}}$ (or from derived quantities such as $\delta\mathcal{H}/\delta x_{\text{pde}}$), so that

$$y_i := \mathcal{M}_i[x_{\text{pde}}], \qquad i = 1, \ldots, N.$$

Let $\mathcal{N}_i$ denote the corresponding injection map that converts the localized reaction $u_i$ into a source term acting on the field dynamics. Together, $(\mathcal{M}_i, \mathcal{N}_i)$ define the local node–field interface at site $i$: $\mathcal{M}_i$ maps field states to node-relevant signals, while $\mathcal{N}_i$ maps node reactions back to localized forcing of the continuum.

Defining the stacked observation vector

$$\mathcal{M}[x_{\text{pde}}] := \begin{pmatrix} \mathcal{M}_1[x_{\text{pde}}] \\ \vdots \\ \mathcal{M}_N[x_{\text{pde}}] \end{pmatrix}, \qquad u := \begin{pmatrix} u_1 \\ \vdots \\ u_N \end{pmatrix},$$

the interconnection can be written compactly as

$$\begin{pmatrix} u_{\text{ode}} \\ y_{\text{ode}} \end{pmatrix} = \Sigma \begin{pmatrix} \mathcal{M}[x_{\text{pde}}] \\ u \end{pmatrix}, \tag{9}$$

where $\Sigma$ is a constant skew-symmetric matrix whose block structure specifies how discrete and field ports are interconnected. For the canonical one-to-one interconnection of Equation (8), $\Sigma$ takes the block-diagonal form

$$\Sigma = \begin{pmatrix} 0 & I_N \\ -I_N & 0 \end{pmatrix},$$

with $I_N$ the $N \times N$ identity matrix.

After interconnection, the discrete port inputs provide an explicit realization of the coupling term $\Phi_i$, while the reaction of the discrete subsystem enters the field dynamics through localized source terms, interface contributions, or dynamic boundary conditions represented abstractly by $\Psi$.

Thus, the pH formalism provides a constructive recipe for the coupling terms that guarantees energy consistency while making explicit how node dynamics, network structure, and field-mediated interactions are combined.

### 4.3 | Mathematical and Numerical Implications

A major strength of the port-Hamiltonian framework is that it does not merely suggest a physically meaningful coupling; it also clarifies when such a coupling is mathematically well defined and how it should be approximated numerically. The choice of observation operator $\mathcal{M}_i$ determines the regularity required of the field $u$. Point evaluation $u(\mathbf{r}_i, t)$ is well defined if $u$ belongs to a space of continuous functions, but for parabolic equations in dimensions $d \geq 2$, solutions with point sources typically lack pointwise continuity [23]. This creates a tension: the field equation may contain delta-function sources $\delta(\mathbf{r} - \mathbf{r}_i)$, yet the node dynamics require evaluating the field at exactly those source locations. In such cases, the coupled system as written may be ill-posed without additional regularization. Common remedies include replacing delta sources with smooth approximations (e.g., Gaussian bumps of finite width), reformulating the coupling through boundary conditions on small excluded volumes, or working in weak formulations where the field is interpreted in a distributional sense. The admissibility of $\mathcal{M}_i$ and $\Psi$ must therefore be assessed together: not every formally appealing coupling yields a well-posed evolution. This issue becomes especially important when moving from formal PDE expressions to well-posed evolution problems in Hilbert spaces [21]. In practice, the pH framework helps identify which interconnections are admissible and which require regularization or a reformulation through boundary variables rather than interior point coupling.

A second important consequence concerns stability and control. Because the interconnection is written directly at the level of power variables, the framework makes it possible to distinguish clearly between conservative exchange, internal dissipation, and external actuation. This is particularly relevant in mixed ODE–PDE settings, where stability depends strongly on the interconnection structure and the chosen feedback law; in coupled fluid–structure port-Hamiltonian models, damping-injection mechanisms are often introduced to obtain the desired closed-loop dissipation properties [24].

Finally, these structural considerations naturally extend to numerical simulation. A naive discretization may destroy the power balance of the continuous model and thereby introduce spurious growth or artificial damping. By contrast, structure-preserving discretizations aim to retain the same energy bookkeeping at the discrete level, so that the finite-dimensional approximation remains passive or dissipative in the same sense as the original system [25, 26]. For the class of problems considered here, this is not merely a numerical convenience but an essential requirement if one wants the discrete model to remain faithful to the physics of the coupled network–field system. For this reason, the numerical treatment of hybrid network–field systems is not simply a matter of discretizing two subsystems separately, but of approximating their interconnection in a way that preserves the relevant balance, passivity, or dissipation properties of the continuous model.

## 5 | Coupled Network–Field Modeling Applications

Sections 3 and 4 introduced the coupled network–field formalism at a generic level, emphasizing its common mathematical structure and the analytical and computational issues it raises. The purpose of the present section is different. Rather than extending the general theory, we show how that abstract structure is instantiated in specific application domains, where the variables, coupling laws, and relevant approximations become system-dependent. In each case, the central question is the same: how can the discrete network dynamics and the evolution of a surrounding continuous medium be written in the form of Equations (1)–(2), and what new phenomena arise from their mutual feedback?

The examples below are therefore not meant to be exhaustive, nor to suggest that all application domains admit the same level of abstraction or analysis. Instead, they serve as representative realizations of the framework, illustrating how a common mathematical backbone accommodates biologically, physically, and technologically distinct systems.

### 5.1 | Neurobiological Examples of Diffusion-Mediated Coupling

A particularly transparent realization of the coupled network–field framework arises in neurobiology, where discrete cellular units communicate through signaling substances that move through the surrounding medium. In such systems, the nodes are individual cells with their own internal dynamics, while the continuous field represents the concentration of a mediating chemical that is released, transported, and removed in space. The key point is that the field is not an externally imposed drive: it is produced by the cells themselves and, in turn, feeds back onto them. Coupling therefore emerges through the dynamics of the medium.

This mechanism is especially natural in circadian synchronization within the suprachiasmatic nucleus (SCN), where individual clock cells exchange signals through diffusible neurochemical cues. At the coarse-grained level, each cell acts both as a dynamical unit and as a source of the shared field. A cell in a given biochemical state secretes signaling molecules into the extracellular medium; those molecules diffuse and degrade; and the resulting local concentration modifies the dynamics of nearby cells. Communication is therefore mediated not by a prescribed pairwise adjacency matrix alone, but by the joint evolution of oscillators and field. The range and strength of the effective interaction are then determined by physical transport properties of the medium, such as diffusivity and degradation rate.

In the notation of Section 2, the SCN model provides a particularly transparent realization of the generic coupled network–field structure. The state $x_i(t)$ of node $i$ represents the phase or internal biochemical configuration of the $i$th clock cell, while the field $u(\mathbf{r}, t)$ denotes the concentration of the diffusing signaling molecule. The field acts back on the cells through a term $\Phi_i(u(\mathbf{r}_i, t), x_i)$, which describes how the local signal sensed at the cell position $\mathbf{r}_i$ modulates its internal dynamics. Conversely, the cells drive the field through source terms $\Psi_i(x_i)$ that encode state-dependent secretion. Diffusion and degradation then determine how that signal spreads across space and how long it persists. In this setting, collective synchronization is an emergent property of the full node–field system.

A concrete example is provided by the SCN model of Silva et al. [27], in which the generic network–field Equations (1)–(2) acquire a direct biological interpretation. Each node variable is the two-dimensional state of the $i$th circadian clock cell,

$$x_i(t) = X_i(t) = \begin{pmatrix} x_i(t) \\ y_i(t) \end{pmatrix},$$

whose intrinsic dynamics is governed by the Kronauer oscillator [28]; thus $F_i(X_i)$ represents the uncoupled circadian dynamics of cell $i$. The continuous field is

$$u(\mathbf{r}, t) = A(\mathbf{r}, t),$$

where $A(\mathbf{r}, t)$ denotes the concentration of a neurotransmitter-like chemical diffusing through the intercellular medium. The feedback from the field to the nodes is local in space and takes the form

$$\Phi_i(u(\mathbf{r}_i, t), X_i) = g(A(\mathbf{r}_i, t)),$$

so that each cell responds to the chemical concentration at its own location. The reciprocal feedback from nodes to field is described by

$$\Psi_j(X_j) = h(X_j),$$

where $h(X_j)$ is the state-dependent secretion rate of the mediating chemical by oscillator $j$. Each oscillator therefore acts as a localized source for the field.

The field itself evolves according to a diffusion–degradation equation with point sources at the cell locations,

$$\varepsilon\, \partial_t A(\mathbf{r}, t) = -\eta A(\mathbf{r}, t) + D\nabla^2 A(\mathbf{r}, t) + \sum_{j=1}^{N} h(X_j)\, \delta(\mathbf{r} - \mathbf{r}_j).$$

This equation has an immediate physical interpretation. The term $D\nabla^2 A$ spreads the signal through space, the term $-\eta A$ removes it through degradation or uptake, and the delta-source sum injects new signal at the positions of the cells. The SCN is thus modeled not as a directly coupled oscillator network, but as a population of oscillators interacting through a shared diffusive medium.

A particularly revealing limit is the fast-diffusion regime, $\varepsilon \ll 1$, in which the field relaxes much faster than the cellular variables. In that case the field can be eliminated adiabatically, yielding

$$A(\mathbf{r}_i) = \sum_{j=1}^{N} \sigma(\mathbf{r}_i - \mathbf{r}_j)\, h(X_j),$$

where $\sigma$ is the Green-function kernel of the operator $\eta - D\nabla^2$. Substituting this expression into the node dynamics [29–31] gives

$$\dot{X}_i = F_i(X_i) + g\left( \sum_{j=1}^{N} \sigma(\mathbf{r}_i - \mathbf{r}_j)\, h(X_j) \right).$$

This reduced form makes the physical content especially transparent: each oscillator feels a weighted superposition of the signals secreted by all others, with weights determined not by an a priori network edge list but by the spatial propagator of the medium. In one spatial dimension, the kernel decays exponentially with distance, so the effective interaction range is set by the competition between diffusion and degradation. Large diffusivity or weak degradation produces longer-ranged coupling and facilitates synchronization over larger distances, whereas strong degradation localizes communication and makes coherent behavior harder to sustain.

Silva et al. [27] showed that this effective range has direct dynamical consequences. Long-ranged coupling promotes both phase and frequency synchronization, while more localized coupling requires stronger interactions and may yield frequency locking without full phase coherence. The biological message is clear: collective circadian order depends not only on the intrinsic properties of individual cells, but also on how efficiently the extracellular medium transports and preserves the signals they exchange.

This line of reasoning was further clarified by Aristides and Viana [32], who derived an integro-differential description for systems with diffusion-mediated coupling and made explicit how nonlocal interaction kernels emerge from the underlying field dynamics. Their work helps formalize a general lesson already visible in the SCN example: once the field is eliminated, one obtains an effective interaction among discrete units, but the structure of that interaction still reflects the physics of transport in the medium.

From a broader circadian perspective, these models connect naturally to earlier and later studies of synchronization in the SCN. Gonze et al. [33] and Bernard et al. [34] showed that population-level rhythmicity can arise through intercellular signaling even when isolated cells are weak or heterogeneous oscillators. Although these models are not always written explicitly in the reaction–diffusion form of Equations (1)–(2), they share the same central mechanism: synchronization is mediated by a collective chemical signal rather than by purely direct pairwise couplings. More recent work has shown that this effective coupling can itself be heterogeneous, state-dependent, or even repulsive. For example, Myung et al. [35] demonstrated that GABA-mediated interactions in the SCN can act repulsively and contribute to seasonal encoding, while Tokuda et al. [36] emphasized the interplay of multiple signaling pathways in maintaining coherent circadian rhythms.

The same basic mechanism reappears, in a less oscillatory but equally instructive form, in neural tissue more generally. Neurons are discrete dynamical units connected by synapses, yet they are also embedded in an extracellular medium through which ions and signaling molecules move [5, 7, 8]. As a result, neural communication is not determined solely by the synaptic wiring diagram: neuronal activity also modifies the ionic and electrical state of the surrounding space, and that modified environment can in turn feed back onto nearby cells through extracellular ion dynamics, ephaptic effects, and diffusive neuromodulation [5–8]. The dynamics is therefore shaped by the interplay between a discrete network of neurons and a continuous field defined in the extracellular medium. In the notation of Section 2, the extracellular neural setting corresponds to node variables $x_i$ describing neuronal state and continuum fields $u(\mathbf{r}, t)$ describing extracellular ionic or chemical concentrations. The observation operators $\mathcal{M}_i$ extract the local extracellular environment sensed by neuron $i$, while $\Phi_i$ describes how that environment modifies excitability and membrane currents. Conversely, $\Psi$ represents the localized release or uptake imbalance through which neuronal activity reshapes the extracellular medium.

Let $x_i(t) \in \mathbb{R}^m$ denote the state of neuron $i$, typically including membrane potential and additional recovery or gating variables, and let the neurons occupy positions $\mathbf{r}_i \in \Omega \subset \mathbb{R}^3$. The extracellular medium supports one or more fields $u(\mathbf{r}, t)$, such as the potassium concentration $[K^+]_e$ or the calcium concentration $[Ca^{2+}]_e$. The neuronal dynamics may then be written as

$$\dot{x}_i = F_i(x_i) + \sum_{j=1}^{N} A_{ij} S(x_j) + \Phi_i(u(\mathbf{r}_i, t), x_i), \tag{10}$$

where $F_i$ describes the intrinsic dynamics of neuron $i$, the term $\sum_j A_{ij} S(x_j)$ represents synaptic input from other neurons, and $\Phi_i$ describes how the local extracellular environment modulates neuronal excitability [37–39]. For example, extracellular potassium alters the potassium reversal potential and hence the ionic currents flowing through the membrane [37, 38]. In that case one may write

$$\Phi_i = g_K \big(V_i - E_K([K^+]_e(\mathbf{r}_i, t))\big). \tag{11}$$

Physically, this means that when potassium accumulates outside the cell, the membrane currents are modified and the neuron can become easier to excite [37, 38]; see Figure 3.

The extracellular field evolves in parallel according to

$$\partial_t u = D\nabla^2 u - \gamma u + \sum_{i=1}^{N} \Psi_i(x_i(t))\delta(\mathbf{r} - \mathbf{r}_i), \tag{12}$$

where $D$ is a diffusion coefficient, $\gamma$ describes uptake, clearance, or decay, and $\Psi_i(x_i)$ gives the rate at which neuron $i$ releases ions or neurotransmitters into the extracellular space [37, 39, 40]. This equation also has a direct physical meaning. The diffusion term spreads the signal through the tissue, the removal term limits how long it persists, and the sum of localized sources injects signal at the positions of active neurons. Each neuron therefore not only responds to its environment but also helps create it.

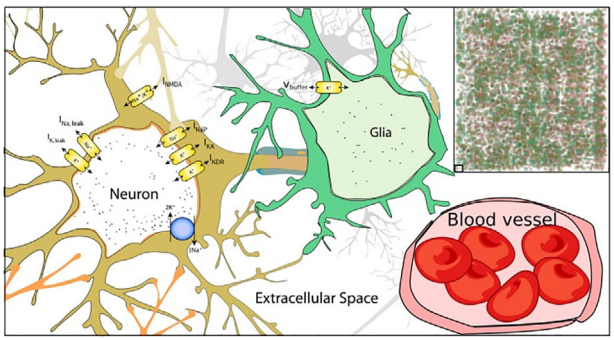


**FIGURE 3** | Neurons (mustard) contain sodium and potassium channels together with the $Na^+/K^+$-ATPase, while dendrites additionally contain NMDA channels. Glial cells (teal) act as potassium buffers, and blood vessels (pink) supply oxygen to support the $Na^+/K^+$-ATPase. Taking the cellular-level model to the continuum limit (upper right) yields a five-compartment model comprising neuronal somata, neuronal dendrites, glia, vasculature, and extracellular space. Reproduced with permission. Ref. [40], Copyright 2025, PLoS.

This feedback loop gives rise to collective effects that neither a purely synaptic network model nor a purely continuum description can capture on its own. A paradigmatic example is spreading depolarization [37, 38, 40], in which a local increase in extracellular potassium depolarizes nearby neurons, promotes further firing and further potassium release, and is then carried through the tissue by diffusion. The result is a slowly propagating wave of disrupted activity, very different from the rapid pulse-like propagation of action potentials [41]. What matters here is that the effective interaction among neurons is no longer determined only by synaptic contacts: it is also shaped by how fast the extracellular signal spreads, how quickly it is removed, and how strongly neurons respond to it [37, 39, 40].

The broader lesson is the same as in the circadian example. Once the field is treated as a dynamical variable, communication among discrete units is mediated by the physics of the surrounding medium. If diffusion is sufficiently fast, the field may sometimes be reduced to an effective nonlocal coupling among neurons. If it is not, then the full coupled node–field description must be retained. In either case, the strength, range, and timescale of the interaction are not imposed a priori, but emerge from transport, degradation, and sensing in the medium itself.

### 5.2 | Infrastructure Networks: Distributed Hazards and Flows

Infrastructure systems can holistically be understood as hybrid discrete–continuous systems. They consist of discrete elements, such as power stations, pumps, road junctions, and terminals, whose states evolve according to an interaction network, but they are embedded in spatial environments where hazards spread out in a continuous fashion. Examples include floodwater over irregular terrain, wind stress along a power corridor, temperature across an urban area, or seismic intensity over a region. Their dynamics therefore cannot be understood from the network alone: the surrounding field loads, damages, or constrains the

infrastructure, while the infrastructure redistributes internal flows and, in some settings, feeds back onto the surrounding field.

A useful formalization distinguishes two coupled layers. The discrete layer is the infrastructure network, with node states $x_i(t)$ representing operational variables such as pressure, flow, voltage, queue length, or equipment status. The continuous layer defines a spatial field $u(\mathbf{r}, t)$ representing the surrounding environment, for example flood depth, hazard intensity, or mechanical stress. Coupling from the field to the network is captured by terms of the form $\Phi_i(u(\mathbf{r}_i, t), x_i)$, which describe how local environmental conditions at the position $\mathbf{r}_i$ of asset $i$ affect its state. Consider, for instance, the additional power burden that heat waves impose on power stations through increased demand for air conditioning in urban areas. Conversely, feedback from the network to the field is encoded through source or sink terms $\Psi(\mathbf{r}, u; \{x_i\})$, representing how infrastructure operation injects, removes, or redistributes mass, energy, or load within the surrounding domain. In the same example, widespread air-conditioning usage produces temperature increases that modify the field's own spatio-temporal dynamics, thereby closing the feedback loop.

Similarly to the neurobiological examples discussed in the previous section, when the relevant spatio-temporal scales align, these network-field couplings can generate phenomena that appear nonlocal when viewed within a single layer, yet follow comparatively simple dynamics when both layers are considered jointly. Such apparent nonlocality in infrastructure systems has been reported to play important, though difficult-to-predict, roles, and existing models often fail to capture its full complexity [42]. Thus, extending the study of infrastructure dynamics to explicitly include coupling with the environment turns out to be a promising direction for future research.

Other particularly relevant examples comprise urban drainage or water-distribution systems exposed to flooding. Here, the network comprises pipes, pumps, tanks, and junctions, while the surrounding field is the water depth over the terrain. A natural node state $x_i(t)$ may include pressure, discharge, and device status. Floodwater acts on the network locally: if the water level at a pump station exceeds a critical threshold, operation may degrade or fail. Within the general formalism, this field-to-node coupling can be represented as

$$\Phi_i(u(\mathbf{r}_i, t), x_i) = -\lambda\, \Theta\big(u(\mathbf{r}_i, t) - h_{\text{crit}}\big)\, x_i, \tag{13}$$

where $\lambda$ is an effective failure rate, and $h_{\text{crit}}$ is a critical inundation depth, and $\Theta$ is the Heaviside step function. In this form, flooding switches the local dynamics from normal operation to rapid degradation once the ambient water depth exceeds the tolerance of the asset. The spatial field therefore does not merely provide background conditions; it actively changes the operability of network components.

The feedback in the opposite direction is equally important. Infrastructure components can act as localized sources, sinks, or transfer points for the field. In the flooding example, leaking pipes, overtopped manholes, or surcharge events exchange water

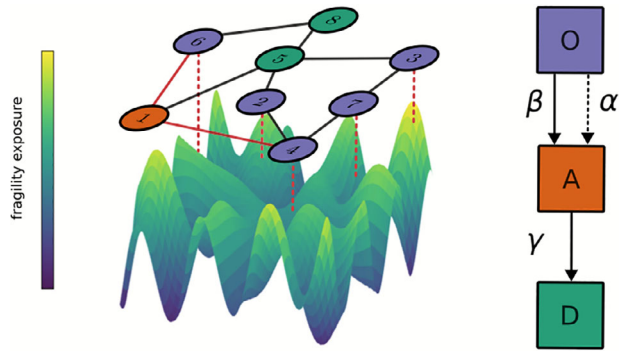


**FIGURE 4** | Schematic representation of the Operational-Affected-Dismantled model. Left: a pictorial representation of how the two local and nonlocal spreading mechanisms of cascade failure act in a toy network. On the one hand, the affected node 1 can spread the failure locally to nodes 4 and 6, through the edges drawn in orange, with rate $\beta$. On the other hand, the nonlocal spreading, which can be seen as mediated by an effective influence field, can cause a long-range spreading between, for example, nodes 2, 3 and 7, which are not direct neighbors of 1. The interactions with the time–dependent, spatially extended hazard field are depicted with red dashed lines, which encodes a further stochastic source for node failure. Right: diagram of the OAD compartmental model. Reproduced with permission. Ref. [43], Copyright 2025, Elsevier.

with the surrounding surface. This can be written schematically as

$$\Psi(\mathbf{r}, u; \{x_i\}) = \sum_{i=1}^{N} \alpha_i(x_i)\, \delta(\mathbf{r} - \mathbf{r}_i), \tag{14}$$

where $\alpha_i(x_i)$ denotes the exchange rate associated with component $i$, and $\delta$ is the Dirac delta function that localizes the exchange at the asset position.

Recent work has explored the effects of the continuous field-like character of natural catastrophes on failure spreading within infrastructure networks [43]. The authors argue that, to evaluate infrastructural risk, it is needed the contribution of both the internal, overload-driven and (possibly) nonlocal dynamics of the infrastructure itself, dubbed the Operational–Affected–Dismantled model in the paper, with exogenous triggers that are modulated by a time-varying, space-dependent hazard field. In this formulation, affected components influence not only their direct neighbors but also the transition rates of distant nodes through the nonlocal mechanism that can be viewed, in turn, as an influence manifold that may not need to follow the architecture of the physical infrastructure; see Figure 4.

This is especially relevant here because it shows how external stressors—such as storms or earthquakes—can be combined with internal spreading dynamics to construct spatial risk maps at arbitrary spatial scale for empirical infrastructures. In the language of the present perspective article, the external catastrophe acts as a spatial field, while the infrastructure state evolves on the discrete network and creates an effective field through nonlocal spreading mechanisms. In this sense, the global field effect of ref. [43] plays a role mathematically analogous to the continuous field $u(\mathbf{r}, t)$ in the general network–field formalism.

A complementary perspective is provided by the multiscale field theory developed in ref. [44], which introduces a hierarchy of descriptions for network flows ranging from mean-field to mesoscopic and full scale-theoretic levels. Although that framework does not model exogenous hazards directly, it is highly relevant here because it provides a principled route from microscopic transport rules on a network to coarse-grained field descriptions. In this way, it broadens the relevance of the network–field viewpoint beyond flooding or cascading failure and points toward a more unified theory of infrastructure flows by offering tools to aggregate node-level information into continuous variables.

These examples also clarify the main challenges in this domain. First, there is often strong scale separation: infrastructure assets are localized and heterogeneous, whereas the relevant hazard or flow field may extend over much larger spatial domains. Second, coupling matters most during extremes—floods, storms, earthquakes, or large disruptions—precisely where observations are sparse, and uncertainty is highest. Third, uncertainty enters through both layers simultaneously, since one must estimate network parameters, environmental forcing, and the exchange terms that connect them. Finally, these systems raise a natural control problem: whether spatial measurements of the field can be assimilated in real time to anticipate failures and regulate the network before local disruptions become systemic.

## 6 | Conclusions

The main contribution of the present perspective article has been to identify shared structural features and to place them within a common conceptual language. By distinguishing between fields posed on network geometries and networks embedded in ambient continua, and by expressing both situations through a common network–field perspective, we have taken a first step toward integrating approaches that are usually developed separately. The aim has not been to erase the important differences among applications, but to isolate the underlying mathematical motifs that recur across them and to show that they can be understood within a single structural framework.

A central challenge that cuts across nearly all coupled network–field systems is empirical identifiability. In many of the settings surveyed here, the variables and mechanisms that mediate the coupling between network and field are only partially observable, and the available measurements are often indirect, coarse-grained, or distributed across incompatible spatial and temporal scales. This creates a double difficulty. On the one hand, there is a modeling problem: how should one decide which coupling mechanisms are physically justified, what should be measured, and what functional forms the interaction terms should take? On the other hand, there is a validation and causality problem: once a hybrid model has been proposed, how can one disentangle the respective contributions of direct network experimentally interactions, field-mediated effects, and external forcing in the observed dynamics? These questions are especially pressing in the application domains discussed in Section 5, where the relevant exchanges often occur through latent or only indirectly accessible variables.

Addressing these challenges will require tighter integration between mathematical theory, measurement, inference, and controlled perturbation. Yet this limited empirical accessibility should not be seen only as an obstacle. Precisely because the key couplings are often hidden, model-driven reasoning has an especially important role to play in identifying plausible mechanisms, guiding what should be measured, and clarifying which coarse-grained descriptions remain faithful to the underlying physics. If this perspective can be pushed further, coupled network–field dynamics may become not merely a collection of specialized models, but a coherent and operational language for spatially embedded complex systems.


### Acknowledgements

C.G., S.G., and A.A. acknowledge support from Ministerio de Ciencia, Innovación y Universidades PID2024-158120NB-C21. O.A. and A.D.G. acknowledge support from Ministerio de Ciencia, Innovación y Universidades PID2024-158120NB-C22. A.A. also acknowledges the ICREA Academia program of Generalitat de Catalunya.


### Conflicts of Interest

The authors declares no conflicts of interest.

### Data Availability Statement

Data sharing not applicable to this article as no datasets were generated or analysed during the current study.

### References


1. M. Barthélemy, "Spatial Networks," *Physics Reports* 499, no. 1–3 (2011): 1–101, https://doi.org/10.1016/j.physrep.2010.11.002.

2. E. Bullmore and O. Sporns, "The Economy of Brain Network Organization," *Nature Reviews Neuroscience* 13, no. 5 (2012): 336–349.

3. M. Kivelä, A. Arenas, M. Barthelemy, J. P. Gleeson, Y. Moreno, and M. A. Porter, "Multilayer Networks," *Journal of Complex Networks* 2, no. 3 (2014): 203–271.

4. H. Barbosa, M. Barthelemy, G. Ghoshal, et al., "Human Mobility: Models and Applications," *Physics Reports* 734 (2018): 1–74.

5. W. Walz, "Role of Astrocytes in the Clearance of Excess Extracellular Potassium," *Neurochemical International* 36, no. 4-5 (2000): 291–300, https://doi.org/10.1016/S0197-0186(99)00137-0.

6. C. A. Anastassiou and C. Koch, "Ephaptic Coupling to Endogenous Electric Field Activity: Why Bother?," *Current Opinion in Neurobiology* 31 (2015): 95–103, https://doi.org/10.1016/j.conb.2014.09.002.

7. B. R. Larsen, A. Stoica, and N. MacAulay, "Managing Brain Extracellular $K^+$ during Neuronal Activity: The Physiological Role of the $Na^+/K^+$-ATPase Subunit Isoforms," *Frontiers in Physiology* Volume 7-2016 (2016), https://doi.org/10.3389/fphys.2016.00141.

8. Ö. D. Özçete, A. Banerjee, and P. S. Kaeser, "Mechanisms of Neuromodulatory Volume Transmission," *Molecular Psychiatry* 29, no. 11 (2024): 3680–3693, https://doi.org/10.1038/s41380-024-02608-3.

9. X. Hu, J. W. Hall, P. Shi, and W. H. Lim, "The Spatial Exposure of the Chinese Infrastructure System to Flooding and Drought Hazards," *Natural Hazards* 80, no. 2 (2016): 1083–1118.

10. Z. Shen, C. Ji, and S. Lu, "Transportation Network Resilience Response to the Spatial Feature of Hazards," *Transportation Research Part D: Transport and Environment* 128 (2024): 104121.

11. E. Mühlhofer, D. N. Bresch, and E. E. Koks, "Infrastructure Failure Cascades Quintuple Risk of Storm and Flood-Induced Service Disruptions

Across the Globe," *One Earth* 7, no. 4 (2024): 714–729, https://doi.org/10.1016/j.oneear.2024.03.010.

12. A. Stéphanou and V. Volpert, "Hybrid modeling in Biology: A Classification Review," *Mathematical modeling of Natural Phenomena* 11, no. 1 (2016): 37–48.

13. G. Ingram, I. Cameron, and K. Hangos, "Classification and Analysis of Integrating Frameworks in Multiscale modeling," *Chemical Engineering Science* 59, no. 11 (2004): 2171–2187.

14. B. Barzel and A.-L. Barabási, "Universality in Network Dynamics," *Nature Physics* 9, no. 10 (2013): 673–681, https://doi.org/10.1038/nphys2741.

15. M. Brio, J.-G. Caputo, and H. Kravitz, "Spectral Solutions of PDEs on Networks," *Applied Numerical Mathematics* 172 (2022): 99–117, https://doi.org/10.1016/j.apnum.2021.09.021.

16. H. Kravitz, M. Brio, and J.-G. Caputo, "Localized Eigenvectors on Metric Graphs," *Mathematics and Computers in Simulation* 214 (2023): 352–372, https://doi.org/10.1016/j.matcom.2023.07.011.

17. L. Böttcher and M. A. Porter, "Dynamical Processes on Metric Networks," *SIAM Journal on Applied Dynamical Systems* 24, no. 4 (2025): 2848–2885.

18. J. Daafouz, M. Tucsnak, and J. Valein, "Nonlinear Control of a Coupled PDE/ODE System Modeling a Switched Power Converter With a Transmission Line," *Systems & Control Letters* 70 (2014): 92–99, https://doi.org/10.1016/j.sysconle.2014.05.009.

19. A. Warsewa, M. Böhm, O. Sawodny, and C. Tarín, "A Port-Hamiltonian Approach to Modeling the Structural Dynamics of Complex Systems," *Applied Mathematical modeling* 89 (2021): 1528–1546, https://doi.org/10.1016/j.apm.2020.07.038.

20. A. J. van der Schaft and B. M. Maschke, "Hamiltonian Formulation of Distributed-Parameter Systems With Boundary Energy Flow," *Journal of Geometry and Physics* 42, no. 1-2 (2002): 166–194, https://doi.org/10.1016/S0393-0440(01)00083-3.

21. Y. Le Gorrec, H. Zwart, and B. Maschke, "Dirac Structures and Boundary Control Systems Associated With Skew-Symmetric Differential Operators," *SIAM Journal on Control and Optimization* 44, no. 5 (2005): 1864–1892, https://doi.org/10.1137/040611677.

22. A. van der Schaft and D. Jeltsema, "Port-Hamiltonian Systems Theory: An Introductory Overview," *Foundations and Trends in Systems and Control* 1, no. 2-3 (2014): 173–378.

23. W. G. Faris, "Partial Differential Equations," (1999), Lecture notes, Department of Mathematics, University of Arizona. Accessed 2026-05-22.

24. F. L. Cardoso-Ribeiro, D. Matignon, and V. Pommier-Budinger, "Modeling by Interconnection and Control by Damping Injection of a Fluid-Structure System With Non-Collocated Actuators and Sensors," in *Proceedings of the International Conference on Noise and Vibration Engineering (ISMA 2016)*.

25. G. Golo, V. Talasila, A. van der Schaft, and B. Maschke, "Hamiltonian Discretization of Boundary Control Systems," *Automatica* 40, no. 5 (2004): 757–771, https://doi.org/10.1016/j.automatica.2003.12.017.

26. H. Egger, O. Habrich, and V. Shashkov, "On the Energy Stable Approximation of Hamiltonian and Gradient Systems," *Computational Methods in Applied Mathematics* 21, no. 2 (2021): 335–349, https://doi.org/10.1515/cmam-2020-0025.

27. F. S. Silva, S. Lopes, and R. Viana, "Synchronization of Biological Clock Cells With a Coupling Mediated by the Local Concentration of a Diffusing Substance," *Communications in Nonlinear Science and Numerical Simulation* 35 (2016): 37–52, https://doi.org/10.1016/j.cnsns.2015.11.003.

28. D. B. Forger, M. E. Jewett, and R. E. Kronauer, "A Simpler Model of the Human Circadian Pacemaker," *Journal of Biological Rhythms* 14, no. 6 (1999): 533–538.

29. Y. Kuramoto and H. Nakao, "Origin of Power-Law Spatial Correlations in Distributed Oscillators and Maps with Nonlocal Coupling," *Physical Review Letters* 76, no. 23 (1996): 4352–4355, https://doi.org/10.1103/PhysRevLett.76.4352.

30. Y. Kuramoto and H. Nakao, "Power-Law Spatial Correlations and the Onset of Individual Motions in Self-Oscillatory Media With Non-Local Coupling," *Physica D: Nonlinear Phenomena* 103, no. 1–4 (1997): 294–313, https://doi.org/10.1016/S0167-2789(96)00264-3.

31. H. Nakao, "Anomalous Spatio-Temporal Chaos in a Two-Dimensional System of Nonlocally Coupled Oscillators," *Chaos: An Interdisciplinary Journal of Nonlinear Science* 9, no. 4 (1999): 902–909, https://doi.org/10.1063/1.166463.

32. R. P. Aristides and R. L. Viana, "An Integro-Differential Equation for Dynamical Systems With Diffusion-Mediated Coupling," *Nonlinear Dynamics* 100 (2020): 3759–3770, https://doi.org/10.1007/s11071-020-05700-9.

33. D. Gonze, S. Bernard, C. Waltermann, A. Kramer, and H. Herzel, "Spontaneous Synchronization of Coupled Circadian Oscillators," *Biophysical Journal* 89, no. 1 (2005): 120–129, https://doi.org/10.1529/biophysj.104.058388.

34. S. Bernard, D. Gonze, B. Čajavec, H. Herzel, and A. Kramer, "Synchronization-Induced Rhythmicity of Circadian Oscillators in the Suprachiasmatic Nucleus," *PLoS Computational Biology* 3, no. 4 (2007): e68, https://doi.org/10.1371/journal.pcbi.0030068.

35. J. Myung, S. Hong, D. DeWoskin, E. De Schutter, D. B. Forger, and T. Takumi, "GABA-Mediated Repulsive Coupling Between Circadian Clock Neurons in the SCN Encodes Seasonal Time," *Proceedings of the National Academy of Sciences of the United States of America* 112, no. 29 (2015): E3920–E3929, https://doi.org/10.1073/pnas.1421200112.

36. I. T. Tokuda, D. Ono, S. Honma, K.-I. Honma, and H. Herzel, "Coherency of Circadian Rhythms in the SCN is Governed by the Interplay of Two Coupling Factors," *PLoS Computational Biology* 14, no. 12 (2018): e1006607, https://doi.org/10.1371/journal.pcbi.1006607.

37. H. C. Tuckwell and R. M. Miura, "A Mathematical Model for Spreading Cortical Depression," *Biophysical Journal* 23 (1978): 257–276.

38. H. Kager, W. J. Wadman, and G. G. Somjen, "Simulated Seizures and Spreading Depression in a Neuron Model Incorporating Interstitial Space and Ion Concentrations," *Journal of Neurophysiology* 84 (2000): 495–512.

39. W. Yao, H. Huang, and R. M. Miura, "A Continuum Neuronal Model for the Instigation and Propagation of Cortical Spreading Depression," *Bulletin of Mathematical Biology* 73 (2011): 2773–2790.

40. J. C. Chang, K. C. Brennan, D. He, et al., "A Mathematical Model of the Metabolic and Perfusion Effects on Cortical Spreading Depression," *PLoS ONE* 8, no. 8 (2013): e70469.

41. G. G. Somjen, "Mechanisms of Spreading Depression and Hypoxic Spreading Depression-Like Depolarization," *Physiological Reviews* 81 (2001): 1065–1096.

42. O. Artime, M. Grassia, M. De Domenico, et al., "Robustness and Resilience of Complex Networks," *Nature Reviews Physics* 6, no. 2 (2024): 114–131.

43. T. Scagliarini, O. Artime, and M. De Domenico, "Assessing the Vulnerability of Empirical Infrastructure Networks to Natural Catastrophes," *Chaos, Solitons & Fractals* 191 (2025): 115813, https://doi.org/10.1016/j.chaos.2024.115813.

44. G. Mikaberidze, O. Artime, A. Díaz-Guilera, and R. M. D'Souza, "Multiscale Field Theory for Network Flows," *Physical Review X* 15, no. 2 (2025): 021044, https://doi.org/10.1103/PhysRevX.15.021044.

## Supporting Information

Additional supporting information can be found online in the Supporting Information section.

**Supporting File:** andp70288-sup-0001-SuppMat.pdf.